Diabetologia
https://doi.org/10.1007/s00125-025-06612-2

ARTICLE

Defective autophagy and AMPK inactivation drive ferroptosis in diabetic kidney disease

Sho Matsui[1] · Takeshi Yamamoto[1] · Yoshitsugu Takabatake[1] · Atsushi Takahashi[1] · Tomoko Namba-Hamano[1] · Jun Matsuda[1] · Satoshi Minami[1] · Shinsuke Sakai[1] · Hiroaki Yonishi[1] · Jun Nakamura[1] · Hideaki Kawai[1] · Takuya Kubota[1] · Isao Matsui[1] · Motoko Yanagita[2,3] · Yoshitaka Isaka[1]

Received: 27 July 2025 / Accepted: 6 October 2025

Abstract

Aims/hypothesis Ferroptosis, a regulated form of cell death characterised by excessive lipid peroxidation, plays a critical role in acute kidney injury (AKI). Individuals with diabetes have an elevated risk of developing AKI. However, the contribution of ferroptosis to the heightened susceptibility to AKI in diabetic kidney disease (DKD) remains unclear. This study aimed to investigate whether DKD influences ferroptosis susceptibility in proximal tubular epithelial cells (PTECs), focusing on autophagy and AMP-activated protein kinase (AMPK) signalling.

Methods We examined the association between ferroptotic signatures and autophagy/AMPK pathways in human kidney biopsy specimens. To explore the roles of autophagy and AMPK in modulating ferroptosis in PTECs during DKD, we subjected streptozocin (STZ)-induced type 1 diabetic mice and type 2 diabetic *db*/*db* mice to ischaemia–reperfusion injury. Primary *Atg5*-deficient and wild-type PTECs were used to further investigate the underlying cellular mechanisms.

Results Analysis of human kidney biopsy specimens revealed an increased ferroptotic signature (4-hydroxynonenal immunostaining), impaired autophagy (SQSTM1 accumulation) and AMPK inactivation (reduced p-AMPK) in PTECs of individuals with DKD. In STZ-treated *Atg5* knockout (Atg5KO) mice, experiments combining ischaemia–reperfusion injury with ferrostatin-1 treatment showed that autophagy suppressed ferroptotic susceptibility. Additionally, susceptibility to ferroptosis was heightened in *db*/*db* mice following ischaemia–reperfusion injury; however, this effect was mitigated by enhancing autophagy through rapamycin treatment. In primary PTECs isolated from Atg5KO mice, ferroptotic cell death and lipid peroxidation were significantly increased, together with elevated mitochondrial reactive oxygen species. Mitochondrial DNA/RNA depletion substantially abolished ferroptotic effects in Atg5KO cells. Furthermore, high-glucose treatment inactivated AMPK and promoted ferroptosis, whereas treatment with the AMPK activator 5-aminoimidazole-4-carboxyamide ribonucleoside (AICAR) attenuated ferroptosis in vitro and reduced vulnerability to AKI in DKD models.

Conclusions/interpretation These findings demonstrate that impaired autophagy and inactivated AMPK heighten susceptibility to ferroptosis in DKD, suggesting that therapeutic strategies targeting autophagy and AMPK activation may reduce ferroptosis-associated kidney injury in individuals with diabetes.

Keywords AMPK · Autophagy · Diabetic kidney disease · Ferroptosis · Mitochondria · Proximal tubules

Sho Matsui and Takeshi Yamamoto contributed equally to this work.

✉ Takeshi Yamamoto
tyamamoto@kid.med.osaka-u.ac.jp

[1] Department of Nephrology, The University of Osaka, Osaka, Japan

[2] Department of Nephrology, Kyoto University Graduate School of Medicine, Kyoto, Japan

[3] Institute for the Advanced Study of Human Biology, Kyoto University, Kyoto, Japan

Abbreviations

4HNE	4-hydroxynonenal
ACC	Acetyl-CoA carboxylase
ACSL4	Acyl-CoA synthetase 4
ACTB	β-Actin
AICAR	5-Aminoimidazole-4-carboxyamide ribonucleoside
AKI	Acute kidney injury
AMPK	AMP-activated protein kinase

Published online: 28 November 2025

Research in context

What is already known about this subject?

- Individuals with diabetes exhibit an increased risk of developing acute kidney injury (AKI)
- Ferroptosis, a regulated form of cell death characterised by excessive lipid peroxidation, plays a critical role in the pathogenesis of AKI
- In diabetes, proximal tubular epithelial cells (PTECs) exhibit impaired autophagy and suppression of AMP-activated protein kinase (AMPK) signalling, a key nutrient-sensing pathway

What is the key question?

- Does diabetic kidney disease (DKD) influence ferroptosis susceptibility in PTECs and, if so, what are the underlying mechanisms?

What are the new findings?

- The ferroptotic signature was elevated in proximal tubules of individuals with DKD, accompanied by impaired autophagy and AMPK inactivation
- Impaired autophagy increased ferroptotic susceptibility by elevating mitochondrial reactive oxygen species in the diabetic kidney
- High glucose-induced AMPK inactivation promoted ferroptosis in PTECs

How might this impact on clinical practice in the foreseeable future?

- Therapeutic strategies that enhance autophagy or activate AMPK may mitigate ferroptosis-related kidney injury in individuals with DKD, offering a potential avenue for renoprotective interventions in diabetes

Atg5KO	*Atg5* knockout
DKD	Diabetic kidney disease
EtBr	Ethidium bromide
Fer-1	Ferrostatin-1
GPX4	Glutathione peroxidase 4
GSEA	Gene set enrichment analysis
HAVCR1/KIM1	Hepatitis A virus cellular receptor 1
HG	High glucose
KAP	Kidney androgen-regulated protein
KEGG	Kyoto Encyclopedia of Genes and Genomes
LG	Low glucose
LRP2/MEGALIN	Low density lipoprotein receptor-related protein 2
MAP1LC3	Microtubule-associated protein light chain 3
mTOR	Mammalian target of rapamycin
NDRG1	N-myc downstream-regulated gene 1
p-ACC	Phosphorylated ACC
p-AMPK	Phosphorylated AMPK
PTEC	Proximal tubular epithelial cell
ROS	Reactive oxygen species
SDH	Succinate dehydrogenase
SQSTM1/p62	Sequestosome 1
STZ	Streptozocin

Introduction

Diabetes affects more than 500 million individuals globally, and this number is projected to rise steadily [1]. Approximately 40% of individuals with diabetes develop diabetic kidney disease (DKD), a complication that can progress to kidney failure requiring dialysis or transplantation, as well as cardiovascular disease and premature mortality [2]. Individuals with diabetes also exhibit an increased risk of acute kidney injury (AKI) [3, 4], and possess reduced renal recovery capacity following AKI [5]. AKI is now widely recognised as a significant risk factor for the onset of chronic kidney disease and eventual kidney failure [6, 7]. Moreover, individuals who experience AKI are at increased risk for long-term morbidity and mortality [8]. Although it is critical that AKI susceptibility is managed in individuals with DKD, the mechanisms responsible for their heightened vulnerability to AKI remain incompletely understood.

Ferroptosis is a regulated form of cell death driven by excessive lipid peroxidation [9]. While it was initially implicated in cancer pathogenesis, ferroptosis has also been linked to a range of non-malignant conditions, including neurodegeneration, liver and lung fibrosis, and autoimmune diseases [10]. Multiple studies have shown

that ferroptotic cell death occurs in proximal tubular epithelial cells (PTECs) [11, 12], which has prompted major advances in ferroptosis research in the kidney that have established ferroptotic cell death in PTECS as a central mechanism in various forms of AKI [13]. However, the role of ferroptosis in increased susceptibility to AKI in DKD remains largely unexplored [14]. Furthermore, the mechanisms driving ferroptosis in this context remain poorly understood.

Our previous research highlighted the critical role of macroautophagy/autophagy, a highly conserved intracellular degradation system that regulates cellular homeostasis [15], in reducing the vulnerability of PTECs to AKI [16, 17]. To investigate this, we used *Atg5* knockout (Atg5KO) mice and cells, as autophagy-related gene 5 (ATG5) binds to ATG12 and ATG16L1, resulting in an E3-like ligase complex that is essential for autophagosome membrane elongation [18]. Furthermore, we demonstrated that type 1 and type 2 diabetes cause dysregulated autophagy in PTECs [19]. While a few studies have suggested that autophagy suppresses ferroptosis via selective autophagic processes such as lysophagy [20], most evidence indicates that autophagy, particularly selective autophagy, participates in the initiation or execution of ferroptosis through targeted degradation of proteins or organelles, giving rise to the concept of 'autophagy-dependent ferroptosis' [21]. For example, one study showed that knockout or knockdown of *Atg5* and *Atg7* limited ferroptosis via nuclear receptor coactivator 4 (NCOA4)-mediated ferritinophagy [22]. Other studies have highlighted roles for various forms of selective autophagy, such as lipophagy, clockophagy and chaperone-mediated autophagy, in promoting ferroptotic cell death through selective degradation of specific proteins or organelles [23–25]. However, given our previous findings that autophagy protects against kidney injury [16, 17], it is conceivable that autophagy may attenuate ferroptotic susceptibility in PTECs. However, the specific impact of autophagy on ferroptosis in PTECs remains unclear.

In diabetes, altered nutrient signalling due to hyperglycaemia contributes to the pathogenesis of DKD [26]. Among these nutrient signals, AMP-activated protein kinase (AMPK), which is activated under energetically stressed conditions in which cellular ATP levels are reduced, has been shown to protect against proximal tubular injury in various diabetic animal models [27, 28]. AMPK plays a central role in reprogramming cellular metabolism from anabolism to catabolism, including the regulation of lipid and glucose metabolism as well as autophagy. AMPK enhances autophagy through multiple mechanisms, primarily by phosphorylating tuberous sclerosis complex 2 (TSC2) and regulatory-associated protein of mammalian target of rapamycin (mTOR) to inhibit mammalian target of rapamycin complex 1 (mTORC1), and by directly activating Unc-51-like autophagy activating kinase 1 (ULK1), which is a key kinase for autophagy induction [29]. However, the role of AMPK in ferroptosis within the diabetic kidney has not been elucidated.

Based on this information, we hypothesised that the diabetic kidney exhibits increased susceptibility to ferroptosis due to impaired autophagy and AMPK inactivation. To test this hypothesis, we investigated the mechanisms by which DKD promotes ferroptosis, focusing on impaired autophagy and AMPK inactivation in the proximal tubules of the streptozocin (STZ)-induced mouse model of type 1 diabetes and the *db*/*db* mouse model of type 2 diabetes.

Methods

Mice *Atg5*$^{F/F}$;kidney androgen-regulated protein (KAP)-Cre and *Atg5*$^{F/F}$;N-myc downstream-regulated gene 1 (NDRG1)-Cre^{ERT2} mice on the C57BL/6 background have been described previously [16, 30, 31]. To generate *Atg5*$^{F/F}$;KAP-Cre (PTEC-specific *Atg5*-deficient mice; hereafter referred to as Atg5KO mice, used for in vivo work) and *Atg5*$^{F/F}$;NDRG1-Cre^{ERT2} (tamoxifen-inducible PTEC-specific *Atg5*-deficient mice, Atg5KO cells used for in vitro work), *Atg5*$^{F/F}$ mice were crossed with the KAP-Cre or NDRG1-Cre^{ERT2} transgenic mice, respectively, at the University of Osaka. B6.BKS(D)-*Lepr*$^{db/db}$/J (*db*/*db*) or B6.BKS(D)-*Lepr*$^{db/+}$/J (*db*/*m*) mice were purchased from CLEA Japan (https://www.jax.org/strain/000697). To induce a type 1 diabetes-like condition, mice were treated with 50 mg/kg STZ (Sigma-Aldrich; S0130) intraperitoneally for four consecutive days at 8 weeks of age. Ferrostatin-1 (Fer-1) (Sigma-Aldrich; SML0583) (5 mg/kg) or vehicle (0.1 ml DMSO [Sigma-Aldrich]/normal saline [154 mmol/l NaCl] at a ratio of 0.01:1) was administered intraperitoneally 30 min before and immediately after ischaemia–reperfusion injury. Rapamycin (LC Laboratories, Woburn, MA, USA; R-5000) (0.4 mg/kg) or vehicle (0.1 ml DMSO/ethanol; 1:1 ratio) was administered intraperitoneally daily for 3 days prior to ischaemia–reperfusion injury. 5-aminoimidazole-4-carboxyamide ribonucleoside (AICAR) (Wako; 2627-69-2) (500 mg/kg) was administered intraperitoneally for 7 days prior to ischaemia–reperfusion injury. Kidney ischaemia was induced and tubular injury was assessed as described previously [31]. In brief, the animals were anaesthetised and kept on a homeothermic table. For unilateral clamping, back incisions were made to expose the kidney pedicles. The pedicles were then clamped for 35 min to induce kidney ischaemia, followed by clamp release for reperfusion. Kidney tubular cells of the cortex were examined by three nephrologists (S. Matsui, J. Nakamura and T. Yamamoto) in a blind manner,

and were scored from 0 to 10 according to the percentage of damaged tubules. Tubular damage was defined as the presence of cell necrosis, which was evaluated in this study by loss of brush border, tubular dilation and cast formation. At least ten high-power fields (×400) were reviewed for each periodic acid–Schiff-stained slide. No animals, samples or data points were excluded from the analysis. All animal procedures were approved by the Animal Research Committee of Osaka University (01-042-018) and complied with the Japanese Animal Protection and Management Law (No. 25).

Cell culture Immortalised wild-type PTEC lines were cultured as previously described [16]. Wild-type PTECs were maintained in low-glucose (LG) DMEM (Nacalai Tesque; 08456-65) supplemented with 5% FBS (Sigma-Aldrich; F7524) at 37°C in a humidified atmosphere of 5% CO_2 and 95% air. Cells were treated with 1 μmol/l erastin2 (Sigma-Aldrich; SML2794), 5 μmol/l Fer-1 (Sigma-Aldrich; SML0583) and 0.5 mmol/l AICAR (Wako; 2627-69-2). To evaluate the effects of high glucose (HG) on AMPK and acetyl-CoA carboxylase (ACC), cells were cultured in LG or HG DMEM (Nacalai Tesque; 16971-55) for 72 h and then treated with AICAR for 24 h before harvest. To evaluate the effects of AMPK on ferroptosis, PTECs were treated with erastin2 in the presence or absence of 5 μmol/l Fer-1 or 0.5 mmol/l AICAR for 24 h. To assess autophagic activity, PTECs were treated with 200 nmol/l bafilomycin A1 (Cayman Chemical; 11038) for 2 h at 37°C before harvest.

Isolation of primary murine renal tubules Primary murine PTECs were isolated from 5-week-old *Atg5*$^{F/F}$ (control cells) or *Atg5*$^{F/F}$;NDRG1-Cre^{ERT2} male mice (hereafter referred to as Atg5KO cells) treated with tamoxifen at 3 weeks of age, as described previously [16] (see electronic supplementary material [ESM] Methods for further details).

Antibodies and reagents Antibodies against the following proteins were used in this study: low density lipoprotein receptor-related protein 2 (LRP2/MEGALIN; a generous gift from T. Michigami, Department of Bone and Mineral Research, Osaka Medical Center and Research Institute for Maternal and Child Health, Japan), sequestosome 1 (SQSTM1/p62; Medical and Biological Laboratory [PM045] for western blotting; Progen [GP62C] for immunostaining), ATG5 (Medical and Biological Laboratory; PM050), microtubule-associated protein light chain 3 (MAP1LC3; Cell Signaling Technology; 2755), β-actin (ACTB; Sigma-Aldrich; A5316), 4-hydroxynonenal (4HNE; Japan Institute for the Control of Aging; MHN-020P), hepatitis A virus cellular receptor 1 (HAVCR1/KIM1; R&D Systems; AF1750), glutathione peroxidase 4 (GPX4) (Abcam; ab125066), acyl-CoA synthetase 4 (ACSL4) (Abcam; ab155282), phosphorylated AMPK (p-AMPK; Cell Signaling Technology; 2535), AMPK (Cell Signaling Technology; 2532), phosphorylated ACC (p-ACC; Cell Signaling Technology; 3661), ACC (Cell Signaling Technology; 3662). The biotinylated secondary antibodies were anti-rabbit IgG (BA-1000), anti-mouse IgG (BA-2001), anti-goat IgG (BA-5000) and anti-guinea pig IgG (BA-7000) (all Vector Laboratories). The horseradish peroxidase-conjugated secondary antibodies were anti-rabbit IgG (P0448) and anti-mouse IgG (P0447) (both DAKO) and the Alexa Fluor-conjugated secondary antibodies were anti-guinea pig Alexa Fluor 488 (A11073), anti-mouse Alexa Fluor 555 (A21422) and anti-rabbit Alexa Fluor 647 (A21245) (all Invitrogen).

Histological analysis Histological analysis was performed as previously described [31]. Antigen retrieval on paraffin-embedded sections, electron microscopy, succinate dehydrogenase (SDH) staining on fresh-frozen sections, and assessment of kidney injury were performed according to established protocols [31, 32]. TUNEL staining was performed using an ApopTag peroxidase in situ apoptosis detection kit (EMD Millipore; S7100). For SDH staining, 5–10 non-overlapping high-power (×400) fields in the cortical region of each kidney section were captured and analysed using NIH ImageJ software [33]. The positively stained area was expressed as a percentage of the total tissue area. For all quantitative or semi-quantitative analyses of histological staining, a minimum of ten high-power fields per kidney were independently reviewed by three nephrologists (S. Matsui, J. Nakamura and T. Yamamoto) in a blinded manner.

Cell death assays Cell death assays were performed in six-well plates. Ferroptosis was induced in primary PTECs and immortalised wild-type PTECs using erastin2 at 20 μmol/l and 1 μmol/l, respectively. At the specified time points, cells (including floating dead cells) were collected and stained with 5 μg/ml propidium iodide. After 15 min, cell viability was evaluated using the Cytek Northern Lights system (Cytek Biosciences) and analysed using FlowJo software (version 10).

Lipid peroxidation analysis To assess lipid peroxidation, cells were stained with 5 μmol/l BODIPY 581/591 C11 in 500 μl HBSS for 10 min at 37°C. The cells were then washed twice with HBSS, and analysed by flow cytometry using the Cytek Northern Lights system equipped with a 488 nm laser.

Assessment of mitochondrial function and biogenesis To evaluate mitochondrial membrane potential, reactive oxygen species (ROS) production and mitochondrial lipid peroxidation, primary PTECs were cultured on 35 mm glass-bottom dishes. Mitochondrial membrane potential was assessed by staining with 50 nmol/l tetramethylrhodamine ethyl ester (Invitrogen) for 30 min at 37°C. Mitochondrial ROS

production was evaluated using 0.3 μmol/l MitoSOX Red (Invitrogen) for 15 min. Mitochondrial lipid peroxidation was measured by incubating cells with 5 μmol/l MitoPerOx (Abcam) for 30 min. Fluorescent images were acquired using an Olympus FV3000 microscope, and the mean fluorescence intensity in fluorescence-positive areas was quantified using ImageJ software. More than five images were obtained for each sample (150 cells per sample).

RNA-seq analysis and bioinformatics Control and Atg5KO cells were treated with 20 μmol/l erastin2 for 24 h before RNA isolation. RNA-seq was performed by the Center of Medical Innovation and Translational Research (Osaka University) and Macrogen Japan. Reads were pre-processed using FastQ Quality Trimmer (version 0.0.14). Trimmed reads were aligned to the reference genome (mm10, GRCm38; https://hgdownload.soe.ucsc.edu/downloads.html) using HISAT2 (version 2.1.0) with default parameters. Read counts for each sample were calculated using FeatureCounts (version 1.4.6). Data normalisation and statistical analysis were performed using the Bioconductor package edgeR (version 3.26.8). Kyoto Encyclopedia of Genes and Genomes (KEGG) pathway gene set enrichment analysis (GSEA) (www.gsea-msigdb.org/gsea/index.jsp) [34, 35] was carried out using gseKEGG in the clusterProfiler package (version 4.6.2) [36]. RNA-seq data were deposited in the NCBI Gene Expression Omnibus (GSE298268).

Kidney biopsy specimens Human kidney specimens were obtained from individuals who underwent kidney biopsy at Osaka University Hospital. Samples with DKD were identified based on pathological criteria for diabetic nephropathy. Non-DKD specimens included samples with no significant pathological abnormalities, benign nephrosclerosis or IgA nephropathy. The extent of SQSTM1/p62 aggregation was quantified as the number of aggregates per centimetre cortical length. The percentage of positively stained areas for 4HNE, SQSTM1/p62, p-AMPK and p-ACC was assessed in at least five randomly selected high-power fields (×400) within the cortex. All immunohistochemical evaluations were independently conducted by three nephrologists (S. Matsui, J. Nakamura and T. Yamamoto) in a blinded manner. All human studies were approved by the Institutional Review Board of Osaka University Hospital (IRB numbers 17334, 20504 and 15234-8). We have complied with all of the relevant ethical regulations, and informed consent was obtained from the individuals who underwent kidney biopsy.

Quantitative real-time PCR Tissue RNA was extracted using TRIzol reagent (Invitrogen) according to the manufacturer's instructions. Real-time SYBR Green PCR analyses (Thermo Fisher Scientific) were performed using a QuantStudio 7 Flex real-time PCR system (Applied Biosystems) to quantify mRNA expression levels in the kidney. The primer sequences used were: *Sdha* (F: 5′- TTACCTGCGTTTCCCCTCAT-3′; R: 5′-AAGTCTGGCGCAACTCAATC-3′), *Pgc1a* (F: 5′-TGATGTGAATGACTTGGATACAGACA-3′; R: 5′-GCTCATTGTTGTACTGG TTGGATATG-3′), *Scad* (F: 5′-TTACCTGGCCTACTCCATCG-3′; R: 5′-TGATCCACTGTTGCTTCTGC-3′), *Lcad* (F: 5′- GCATCAACATCGCAGAGAAA-3′; R: 5′-ACGCTTGCTCTTCCCAAGTA-3′), *Vlcad* (F: 5′- GCATCTTGCTCTATGGCACA-3′; R: 5′-CACTCGAGGGCTCTGTTAGG-3′), *mtCo2* (F: 5′-ATAATCCCAACAAACGACCT-3′; R: 5′-CTCGGTTATCAACTTCTAGCA-3′), *mtNd1* (F: 5′-CTAGCAGAAACAAACCGGGC-3′; R: 5′-CCGGCTGCGTATTCTACGTT-3′), *mtActb* (F: 5′-ACCGTGAAAAGATGACCCAG-3′; R: 5′-AGCCTGGATGGCTACGTACA-3′) and *Actb* (F: 5′-TGACAGGATGCAGAAGGAGA-3′; R: 5′-ACATCTGCTGGAAGGTGGAC-3′) (F, forwards; R, reverse).

Western blot analysis Western blot analyses were performed as previously described [37]. Briefly, proteins were extracted using Cell Lysis Buffer (Cell Signaling Technology; 9803) with complete protease inhibitor cocktail (Roche; 11697498001), separated by SDS–PAGE, and then transferred to PVDF membranes (GE Healthcare). We used 10–20% gradient gels to detect proteins of low molecular mass such as MAP1LC3.The membranes were blocked in a blocking solution comprising 1.0% BSA in TBS containing 0.1% Tween-20, and incubated with primary antibodies overnight at 4°C. After being washed, the membranes were incubated with secondary antibodies for 1 h at room temperature. After additional washes, chemiluminescent signals

Table 1 Characteristics of individuals with or without DKD whose kidney sections were used for immunostaining

	Non-DKD (*n*=16)	DKD (*n*=16)	
Age (years)	53.5 ± 18.7	56.3 ± 15.2	
Female sex (%)	4 (25%)	2 (12.5%)	
Creatinine (μmol/l)	98 ± 16	114 ± 35	
eGFR (ml/min per 1.73 m^2)	54.5 ± 15.1	51.3 ± 22.1	
Urinary protein (g/gCr)	1.65 ± 1.25	2.62 ± 2.25	
BMI (kg/m^2)	22.9 ± 2.9	24.6 ± 3.6	
HbA_{1c} (mmol/mol)	36.4 ± 4.4	49.4 ± 6.4*	
HbA_{1c} (%)	5.48 ± 0.40	6.67 ± 0.58*	
RPS classification (*n*)		Class I	4
		Class IIa	3
		Class IIb	6
		Class III	3

Values for continuous variables are presented as mean ± SD; those for categorical variables are *n* (%)

Profiles were compared between the groups : *p<0.05 vs non-DKD

RPS, Renal Pathology Society

were detected using an enhanced chemiluminescence reagent (Clarity Western ECL Substrate, Bio-Rad; 1705061). Images were obtained using ChemiDoc Touch (Bio-Rad).

Establishment of Rho^0 renal tubule cells Renal tubule cells were cultured in DMEM/F12 medium supplemented with 100 ng/ml ethidium bromide (EtBr) (Bio-Rad; 161-0433), 50 µg/ml uridine (Sigma-Aldrich; U3750) and 1 mmol/l sodium pyruvate (Gibco; 11360070) for 8 days to generate mtDNA- or mtRNA-depleted cells (Rho^0 phenotype). The depletion of mtRNA was confirmed by quantitative real-time PCR. No overt cell death was observed following EtBr treatment; however, cell proliferation was reduced compared with untreated cells.

Statistical analysis All data are presented as means ± SD. Statistical analyses were performed using JMP software version 17.2.0 (SAS Institute). Group comparisons were evaluated using one-way ANOVA followed by post hoc Tukey–Kramer testing. Comparisons between two groups were performed using an unpaired Student's *t* test where appropriate. Statistical significance was defined as $p<0.05$.

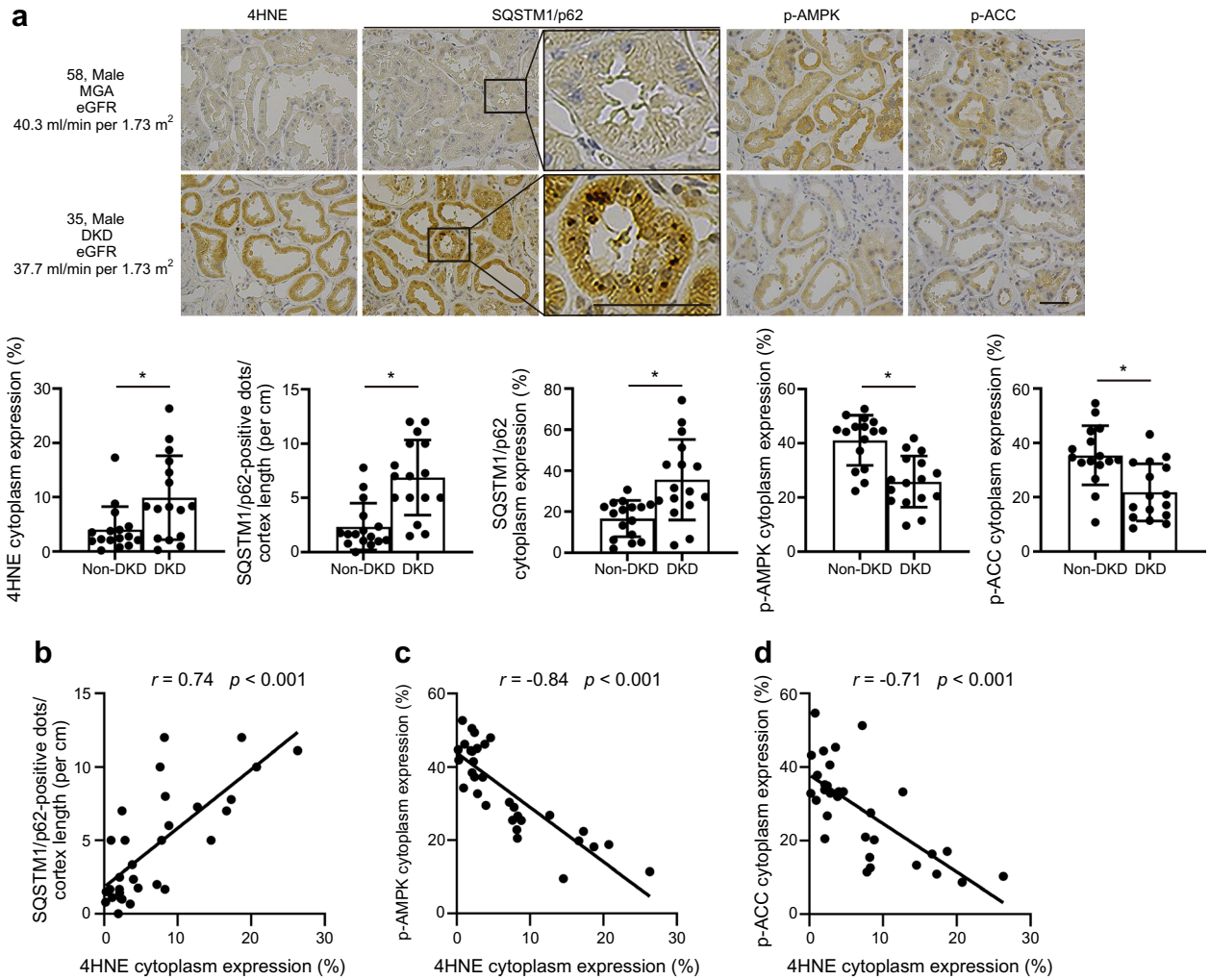

Fig. 1 The ferroptotic signature is increased in PTECs from individuals with DKD. (**a**) Representative immunohistochemical images showing 4HNE, SQSTM1/p62, p-AMPK and p-ACC staining in kidney biopsy samples from individuals with or without DKD, together with their corresponding age, sex, aetiology and eGFR (ml/min per 1.73 m^2). Haematoxylin was used for counterstaining. Scale bars, 50 µm. Regions exhibiting positive immunostaining are shown. The number of SQSTM1/p62-positive aggregates per unit cortex length was quantified. (n=16 per group). (**b**–**d**) Correlation of the 4HNE-positive PTEC area with SQSTM1/p62 aggregate count (**b**), p-AMPK-positive PTEC area (**c**), and p-ACC-positive PTEC area (**d**). Relationships were assessed using Pearson's correlation with corresponding p values. Data are means ± SD. Statistically significant differences are indicated by asterisks ($p<0.05$). MGA, minor glomerular abnormalities

Results

Ferroptosis signature is increased in PTECs of individuals with DKD We first examined whether PTECs from individuals with DKD exhibit an enhanced ferroptosis signature, impaired autophagy and AMPK inactivation compared with those from individuals without DKD. No significant differences were observed for age, eGFR, urinary protein levels or BMI between the two groups. However, HbA_{1c} levels were elevated in the DKD group (Table 1). The histological severity of diabetic nephropathy, as assessed by the Renal Pathology Society classification, ranged from class I to class III (Table 1). Lipid peroxide accumulation was evident in PTECs from DKD individuals, as indicated by increased 4HNE expression (Fig. 1a). Additionally, expression of GPX4 protein, a well-established ferroptosis-associated biomarker [38], was significantly downregulated in DKD PTECs and inversely correlated with 4HNE expression (ESM Fig. 1a, b). Furthermore, impaired autophagy and AMPK inactivation were evident in DKD PTECs, as indicated by SQSTM1/p62 accumulation and reduced p-AMPK expression, respectively (Fig. 1a). Notably, 4HNE expression was positively correlated with SQSTM1/

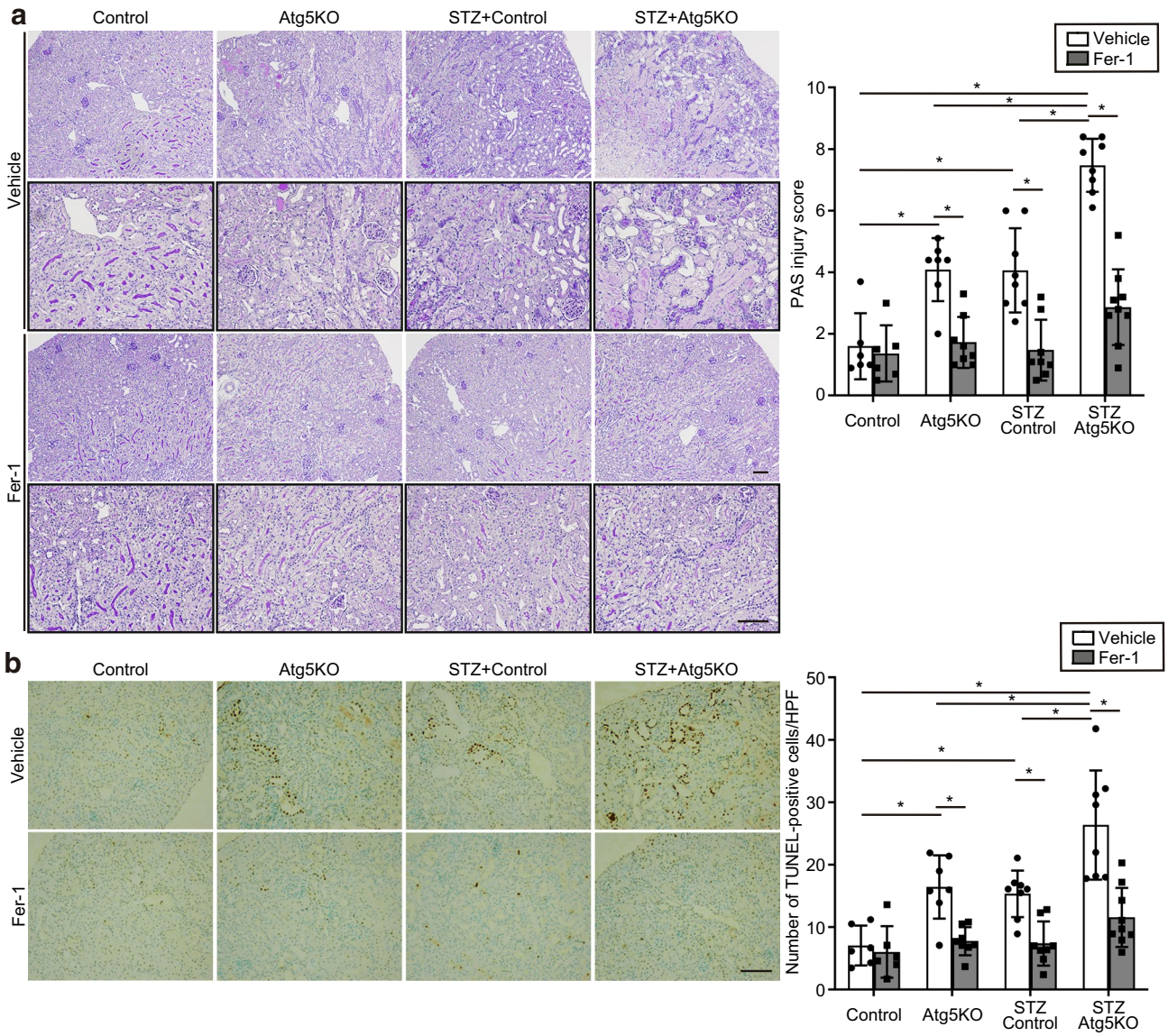

Fig. 2 Autophagy reduces vulnerability to ferroptosis in the kidneys of STZ-treated mice. Saline- or STZ-treated control and Atg5KO mice were subjected to unilateral ischaemia–reperfusion injury, followed by treatment with either vehicle or Fer-1. (**a**) PAS and (**b**) TUNEL staining of the ischaemia–reperfusion-injured renal cortex (n=6–9 per group). PAS injury scores are shown. TUNEL-positive PTECs were quantified across at least ten high-power fields (HPF) (×200). Scale bars, 100 μm. Data are means ± SD. Statistically significant differences are indicated by asterisks (p<0.05). All images are representative of multiple experiments. PAS, periodic acid–Schiff

p62 accumulation and negatively correlated with p-AMPK expression (Fig. 1b). Collectively, these findings indicate that ferroptosis is elevated in PTECs of individuals with DKD. Given the observed correlations between ferroptosis markers, autophagy impairment and AMPK inactivation, we further explored the potential mechanistic links among these factors in the context of DKD.

Autophagy suppresses ferroptosis susceptibility in type 1 diabetic kidneys We next investigated whether autophagy impairment increases ferroptosis susceptibility in PTECs in vivo. Our previous study demonstrated that autophagic activity in nephropathy differs between models of type 1 and 2 diabetes, and that, in type 1 diabetic nephropathy, elevated basal autophagic activity induces lysosomal stress, ultimately leading to autophagic stagnation (ESM Fig. 2) [19]. To assess the combined effects of type 1 diabetes and dysregulated autophagy on ferroptosis, we treated 8-week-old $Atg5^{F/F}$ mice (control mice) and Atg5KO mice with STZ or vehicle. At 12 weeks of age, the mice were subjected to ischaemia–reperfusion injury, a well-established model of ferroptosis induction in PTECs [12]. To evaluate the

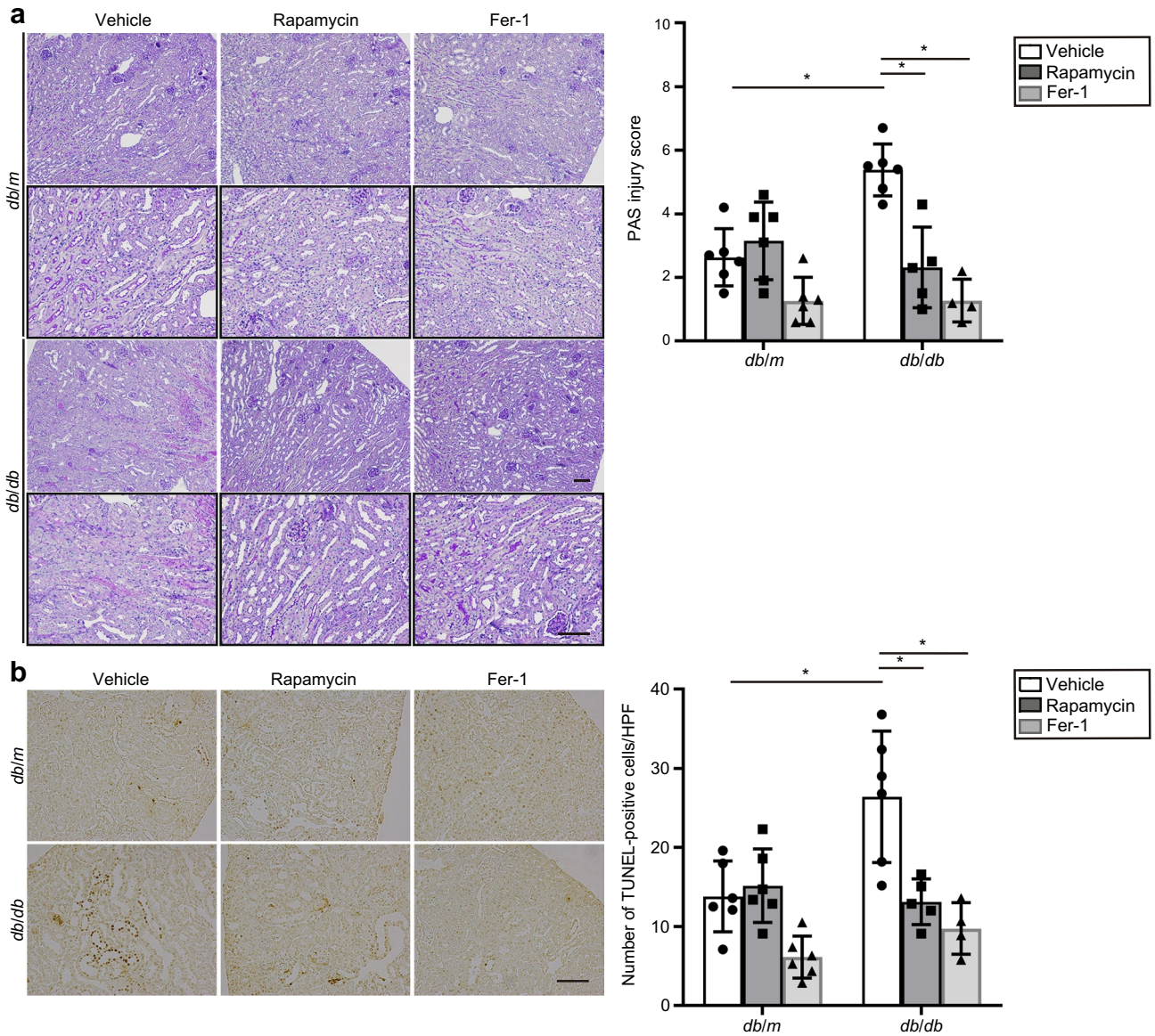

Fig. 3 Improving autophagy reduces susceptibility to ferroptosis in *db/db* mouse kidneys. *db/m* and *db/db* mice were treated with vehicle, rapamycin or Fer-1, and subjected to unilateral ischaemia–reperfusion injury. (**a**) PAS and (**b**) TUNEL staining of ischaemia–reperfusion-injured kidney cortices (n=4–6 per group). The PAS injury score is indicated. TUNEL-positive PTECs were quantified in a minimum of ten high-power fields (HPF) (×200). Scale bars, 100 μm. Data are means ± SD. Statistically significant differences are indicated by asterisks (p<0.05). All images are representative of multiple experiments. PAS, periodic acid–Schiff

contribution of ischaemia–reperfusion-induced ferroptosis in DKD, either vehicle or the ferroptosis inhibitor Fer-1 were administered. Compared with control mice, STZ-treated control mice and vehicle-treated Atg5KO mice exhibited severe tubular injury, characterised by extensive cellular debris (Fig. 2a). This injury was further exacerbated in STZ-treated Atg5KO mice. The number of TUNEL-positive tubular cells, as well as 4HNE and HAVCR1/KIM-1 expression in

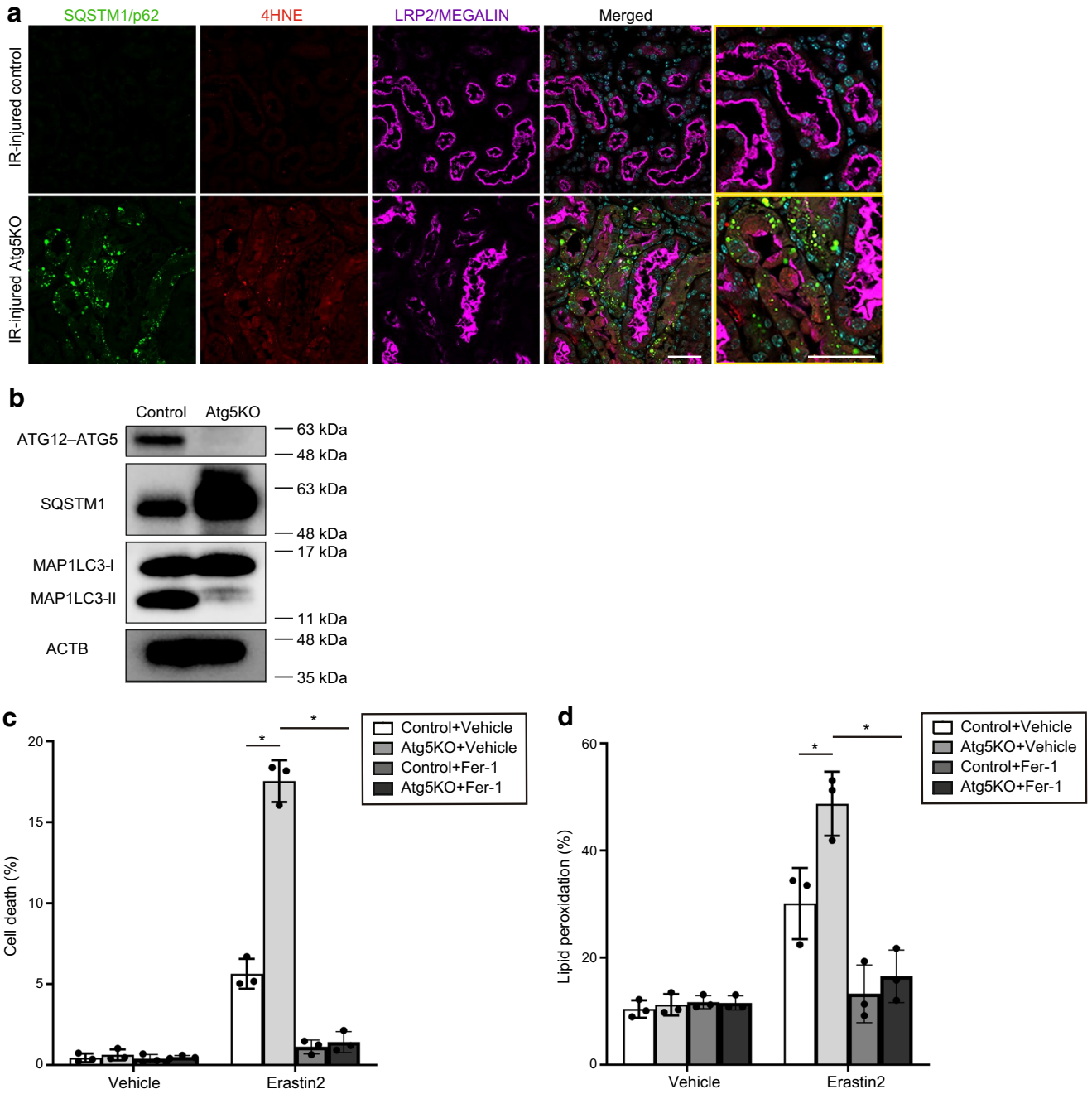

Fig. 4 Autophagy inhibits ferroptotic cell death in PTECs. (**a**) Representative immunofluorescence images showing SQSTM1/p62 (green), 4HNE (red) and LRP2/MEGALIN (purple) staining in the renal cortex of ischaemia–reperfusion-injured control and Atg5KO mice (n=6–7 per group). Scale bars, 50 μm. (**b**) Representative western blot images of ATG12–ATG5, SQSTM1 and MAP1LC3 in control and Atg5KO cells. Autophagy deficiency was confirmed by reduced ATG5 expression, accumulation of SQSTM1/p62, and impaired conversion of MAP1LC3-I to MAP1LC3-II (n=3 per group). β-Actin (ACTB) was used as the loading control. (**c**, **d**) Quantification of cell death (**c**) and lipid peroxidation (**d**) in control and Atg5KO cells treated with or without 20 μmol/l erastin2 for 48 h. Data are means ± SD. Statistically significant differences are indicated by asterisks (p<0.05). All images are representative of multiple experiments. IR, ischaemia–reperfusion

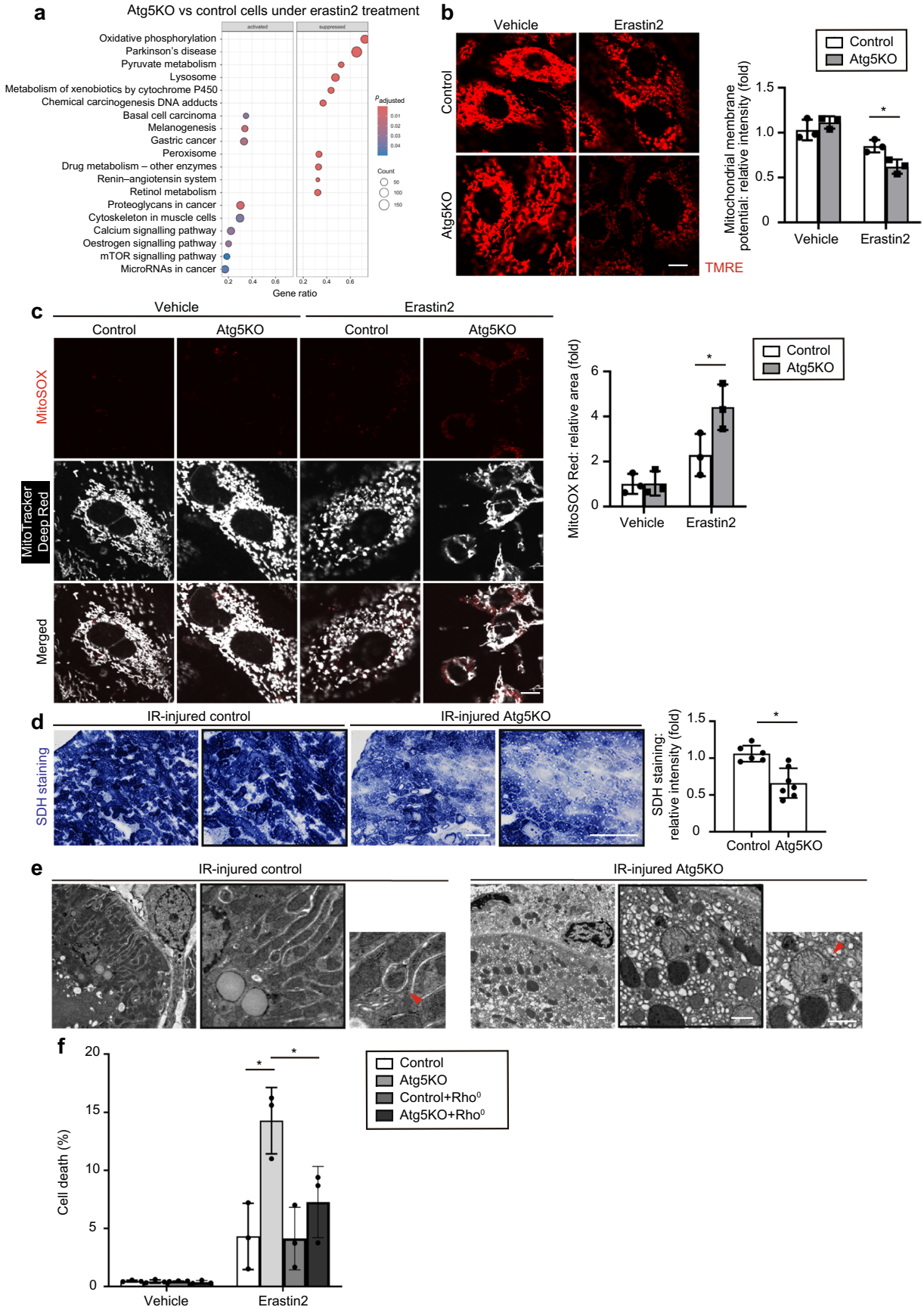
a
Atg5KO vs control cells under erastin2 treatment
activated
suppressed
Oxidative phosphorylation
Parkinson's disease
Pyruvate metabolism
Lysosome
Metabolism of xenobiotics by cytochrome P450
Chemical carcinogenesis DNA adducts
Basal cell carcinoma
Melanogenesis
Gastric cancer
Peroxisome
Drug metabolism – other enzymes
Renin–angiotensin system
Retinol metabolism
Proteoglycans in cancer
Cytoskeleton in muscle cells
Calcium signalling pathway
Oestrogen signalling pathway
mTOR signalling pathway
MicroRNAs in cancer
0.2
0.4
0.6
Gene ratio
Padjusted
0.01
0.02
0.03
0.04
Count
50
100
150
b
Vehicle
Erastin2
Control
Atg5KO
TMRE
Control
Atg5KO
Mitochondrial membrane potential: relative intensity (fold)
1.5
1.0
0.5
0
*
Vehicle
Erastin2
c
Vehicle
Erastin2
Control
Atg5KO
Control
Atg5KO
MitoSOX
MitoTracker Deep Red
Merged
MitoSOX Red: relative area (fold)
6
4
2
0
*
Control
Atg5KO
Vehicle
Erastin2
d
IR-injured control
IR-injured Atg5KO
SDH staining
SDH staining: relative intensity (fold)
1.5
1.0
0.5
0
*
Control
Atg5KO
e
IR-injured control
IR-injured Atg5KO
f
Cell death (%)
20
15
10
5
0
*
*
Control
Atg5KO
Control+Rho0
Atg5KO+Rho0
Vehicle
Erastin2

◂**Fig. 5** Loss of *Atg5* exacerbates mitochondrial dysfunction and ROS in PTECs. (**a**) RNA-seq transcriptomic analysis was performed on control and Atg5KO cells treated with erastin2 for 24 h to identify significantly enriched pathways (n=3) and KEGG pathway GSEA was carried out. (**b**, **c**) Mitochondrial membrane potential (**b**) and mitochondrial ROS production (**c**) in control and Atg5KO cells treated with vehicle or erastin2 were assessed using tetramethylrhodamine ethyl ester (TMRE) and MitoSOX Red staining, respectively. Quantitative data for relative signal intensity are presented. Over 150 cells were analysed per condition. (**d**) Representative images of SDH staining in the renal cortex of ischaemia–reperfusion-injured control and Atg5KO mouse kidney cortices (n=6–7 per group). Relative staining intensities are shown. (**e**) Electron microscopy images of ischaemia–reperfusion-injured kidneys of control and Atg5KO mice. The red arrowhead in control mouse kidneys indicates mitochondria enclosed within an autophagosome, while the red arrowhead in Atg5KO mouse kidneys indicates outer mitochondrial membrane rupture (n=3 per group). (**f**) Quantification of cell death in control, Atg5KO, control + Rho^0 and Atg5KO + Rho^0 cells treated with or without 20 μmol/l erastin2 for 48 h. Scale bars, 10 μm (**b**, **c**), 100 μm (**d**) and 1 μm (**e**). Data are means ± SD. Statistically significant differences are indicated by asterisks (p<0.05). All images are representative of multiple experiments. IR, ischaemia–reperfusion

PTECs following ischaemia–reperfusion injury, correlated with the extent of tubular damage (Fig. 2b and ESM Fig. 3a, b). Notably, Fer-1 administration ameliorated kidney injury in STZ-treated control mice, vehicle-treated Atg5KO mice and STZ-treated Atg5KO mice, with no significant differences in injury observed among the Fer-1-treated groups (Fig. 2a, b and ESM Fig. 3a, b). These findings suggest that autophagy mitigates ferroptosis susceptibility in the kidneys of type 1 diabetic mice.

Improving autophagy suppresses susceptibility to ferroptosis in type 2 diabetic kidneys To evaluate the significance of ischaemia–reperfusion-induced ferroptosis in the kidneys of type 2 diabetic mice, in which autophagic activity is suppressed via mTOR signalling due to elevated plasma insulin levels (ESM Fig. 2) [19], we subjected 12-week-old *db*/*m* and *db*/*db* mice to ischaemia–reperfusion injury. Severe tubular injury, marked by abundant cellular debris, was observed in ischaemia–reperfusion-injured *db*/*db* mice but was attenuated by Fer-1 treatment (Fig. 3a). Additionally, treatment with rapamycin, which enhances autophagy by inhibiting mTOR signalling, ameliorated tubular injury in *db*/*db* mice. The number of TUNEL-positive tubular cells, together with 4HNE and HAVCR1/KIM-1 expression in PTECs following ischaemia–reperfusion injury, paralleled the extent of tubular damage (Fig. 3a, b and ESM Fig. 3c, d). These findings indicate that improving autophagy suppresses susceptibility to ferroptosis in *db*/*db* mice.

Atg5 deficiency sensitises PTECs to ferroptotic cell death To confirm whether ischaemia–reperfusion-induced ferroptosis occurs in autophagy-deficient PTECs in vivo, we analysed 4HNE expression and SQSTM1/p62 accumulation in ischaemia–reperfusion-injured control and Atg5KO mice. Although 4HNE expression and SQSTM1/p62 accumulation were minimal in ischaemia–reperfusion-injured control mice, 4HNE expression was markedly increased in autophagy-deficient PTECs, as indicated by the occurrence of SQSTM1/p62-positive PTECs in ischaemia–reperfusion-injured Atg5KO mice (Fig. 4a).

To further investigate the role of autophagy in ferroptosis in PTECs, we isolated renal proximal tubule cells from $Atg5^{F/F}$ mice (hereafter referred to as control cells) and $Atg5^{F/F}$;NDRG1 mice (tamoxifen-inducible PTEC-specific *Atg5*-deficient, hereafter referred to as Atg5KO cells). Cells were treated with the ferroptosis inducer erastin2. The *Atg5* deficiency in Atg5KO cells was confirmed by reduced ATG5 expression, impaired MAP1LC3-I to MAP1LC3-II conversion, and SQSTM1/p62 accumulation (Fig. 4b). Atg5KO cells exhibited significantly increased susceptibility to erastin2-induced ferroptotic cell death and lipid peroxidation (Fig. 4c, d). Ferroptotic cell death and lipid peroxidation were completely suppressed by Fer-1 in control and Atg5KO cells (Fig. 4c, d). Collectively, these findings demonstrate that autophagy suppresses ferroptosis susceptibility in PTECs.

Autophagy inhibits ferroptosis by reducing mitochondrial ROS We found that autophagy does not influence several well-established ferroptosis mechanisms, including the expression of the key ferroptosis-regulatory proteins ACSL4 and GPX4 (ESM Fig. 4). To explore the mechanisms by which *Atg5* deficiency sensitises PTECs to ferroptosis, control and Atg5KO cells were treated with erastin2 and subjected to RNA-seq transcriptomic analysis. GSEA revealed a significant downregulation of the KEGG pathway 'oxidative phosphorylation' in Atg5KO cells (Fig. 5a). The kidney has the second-highest mitochondrial content and oxygen consumption after the heart [39]. Moreover, it is one of the most mitophagy-enriched organs [40], where damaged and depolarised mitochondria are selectively removed and recycled to maintain mitochondrial function [41]. Based on the reduced oxidative phosphorylation observed in Atg5KO cells and the critical role of mitophagy in maintaining renal mitochondrial homeostasis, we next focused on mitochondrial alterations in PTECs.

Upon erastin2 treatment, Atg5KO cells exhibited reduced mitochondrial membrane potential and increased mitochondrial ROS, as assessed by tetramethylrhodamine ethyl ester and MitoSOX Red staining, respectively (Fig. 5b, c). Additionally, mitochondrial lipid peroxidation, as indicated by MitoPerOx staining [42], was markedly elevated in Atg5KO cells under erastin2 treatment (ESM Fig. 5a).

Consistently, mitochondrial respiratory activity, as assessed by SDH staining, was significantly reduced in the kidneys of ischaemia–reperfusion-injured Atg5KO mice compared with ischaemia–reperfusion-injured kidneys of control mice (Fig. 5d). Electron microscopy of ischaemia–reperfusion-injured kidneys of control mice showed preserved mitochondrial morphology and mitophagy, characterised by mitochondria enclosed within autophagosomes, in PTECs (Fig. 5e and ESM Fig. 5b). In contrast, ischaemia–reperfusion-injured kidneys of Atg5KO mice exhibited an absence of autophagosomes and severe mitochondrial abnormalities, including smaller mitochondria with increased membrane density, cristae loss and outer membrane rupture, features that are consistent with ferroptotic morphology (Fig. 5e and ESM Fig. 5b). These findings suggest that autophagy deficiency exacerbates mitochondrial dysfunction-induced ferroptosis.

To determine whether autophagy suppresses ferroptosis by reducing mitochondrial ROS, we established primary Rho^0 cells by culturing PTECs in the presence of EtBr for 8 days. The absence of mitochondrial DNA was confirmed by negligible transcript levels of *Co2* and *Nd1* following EtBr treatment (ESM Fig. 6). There was no significant difference in ferroptotic cell death between vehicle-treated control cells and Rho^0 control cells under erastin2 treatment. However, compared with vehicle-treated Atg5KO cells, ferroptotic cell death was significantly reduced in Rho^0 Atg5KO cells under erastin2 treatment (Fig. 5f). Collectively, these findings suggest that autophagy protects against ferroptosis by mitigating mitochondrial ROS accumulation in PTECs.

HG-induced inactivation of AMPK promotes ferroptosis in PTECs Next we investigated whether HG influences AMPK, a central energy regulator, and whether its altered activity contributes to ferroptosis. In cultured PTECs, HG treatment led to reduced p-AMPK expression (Fig. 6a). AMPK regulates lipid metabolism by directly phosphorylating ACC1 and ACC2, thereby suppressing fatty acid synthesis and promoting fatty acid oxidation via activation of carnitine palmitoyltransferase 1 (CPT1) through relief of malonyl-CoA-mediated inhibition at the mitochondrial outer membrane [43]. As a downstream target of AMPK, p-ACC expression was significantly reduced following HG treatment (Fig. 6a). Additionally, HG treatment decreased the mRNA levels of fatty acid oxidation-related genes, including *Cpt1a* (ESM Fig. 7). Furthermore, HG treatment enhanced ferroptotic cell death and lipid peroxidation under erastin2 treatment (Fig. 6b, c). In human kidney biopsy specimens, p-ACC expression was suppressed in PTECs from individuals with DKD (Fig. 1a). Notably, p-ACC expression was positively correlated with p-AMPK expression and negatively correlated with 4HNE expression in PTECs (Fig. 1d and ESM Fig. 1b). These findings suggest that AMPK activation may play a protective role against HG-induced ferroptosis.

To determine whether HG promotes ferroptosis via AMPK inactivation, we treated PTECs with the AMPK activator AICAR. AICAR restored HG-induced reductions in p-AMPK and p-ACC expression (Fig. 6a and ESM Fig. 7) and significantly attenuated HG-induced ferroptotic cell death and lipid peroxidation under erastin2 treatment (Fig. 6d). Collectively, these findings indicate that HG promotes ferroptosis by disrupting the AMPK–ACC axis.

Given the role of AMPK in regulating autophagy, we further investigated whether AICAR ameliorates HG-induced impairment of autophagy. HG increased the protein levels of SQSTM1/p62 compared with LG, indicating that HG induces autophagy impairment (ESM Fig. 8a). Next, we assessed the autophagic flux index, defined as the proportions of MAP1LC3-II in the presence or absence of bafilomycin A1. AICAR enhanced autophagic flux in HG-treated PTECs (ESM Fig. 8b). These findings suggest that HG-induced AMPK dysfunction disrupts not only ACC phosphorylation but also autophagy activity.

AMPK activation attenuates ischaemia–reperfusion injury susceptibility in diabetic mice Based on our in vitro findings, we further examined the role of AMPK in in vivo DKD models. Consistent with our in vitro results, type 1 and type 2 diabetic mice exhibited reduced p-AMPK and p-ACC expression compared with non-diabetic controls (Fig. 7a). We then investigated whether AMPK activation mitigates susceptibility to ischaemia–reperfusion-induced ferroptosis in diabetic mice. Kidney injury severity and the number of TUNEL-positive tubular cells were significantly increased in ischaemia–reperfusion-injured STZ-treated and *db*/*db* mice compared with ischaemia–reperfusion-injured non-diabetic controls (Fig. 7b, c). The effect of this injury was significantly attenuated by AICAR treatment in both diabetic models. Furthermore, AICAR suppressed lipid peroxidation and reduced tubular injury in diabetic kidneys (Fig. 7d, e). These findings suggest that AMPK activation enhances resistance to ferroptosis and protects against ischaemia–reperfusion-induced kidney injury in diabetic mice.

Discussion

In this study, we found that the ferroptotic signature in PTECs was elevated in individuals with DKD, accompanied by impaired autophagy and AMPK inactivation. We also demonstrated that type 1 and type 2 diabetes sensitised PTECs to ferroptosis through distinct mechanisms. First,

impaired autophagy increased susceptibility to ferroptosis by elevating mitochondrial ROS. Second, HG-induced AMPK inactivation promoted ferroptosis. These mechanisms may underlie the heightened ferroptotic vulnerability observed in DKD mice. A schematic summary is provided in Fig. 8.

Our analysis of human kidney samples revealed that the ferroptotic signature was elevated in PTECs of individuals with DKD, positively correlating with dysregulated autophagy and negatively correlating with AMPK activity. These findings indicate that increased ferroptosis sensitisation occurs not only in DKD mouse models but also in human DKD, probably driven by autophagy dysfunction and AMPK inactivation. Although we assessed lipid peroxide accumulation rather than ferroptosis itself in human samples, membrane lipid peroxidation is a critical event in the execution of ferroptosis [44], and is therefore a valid

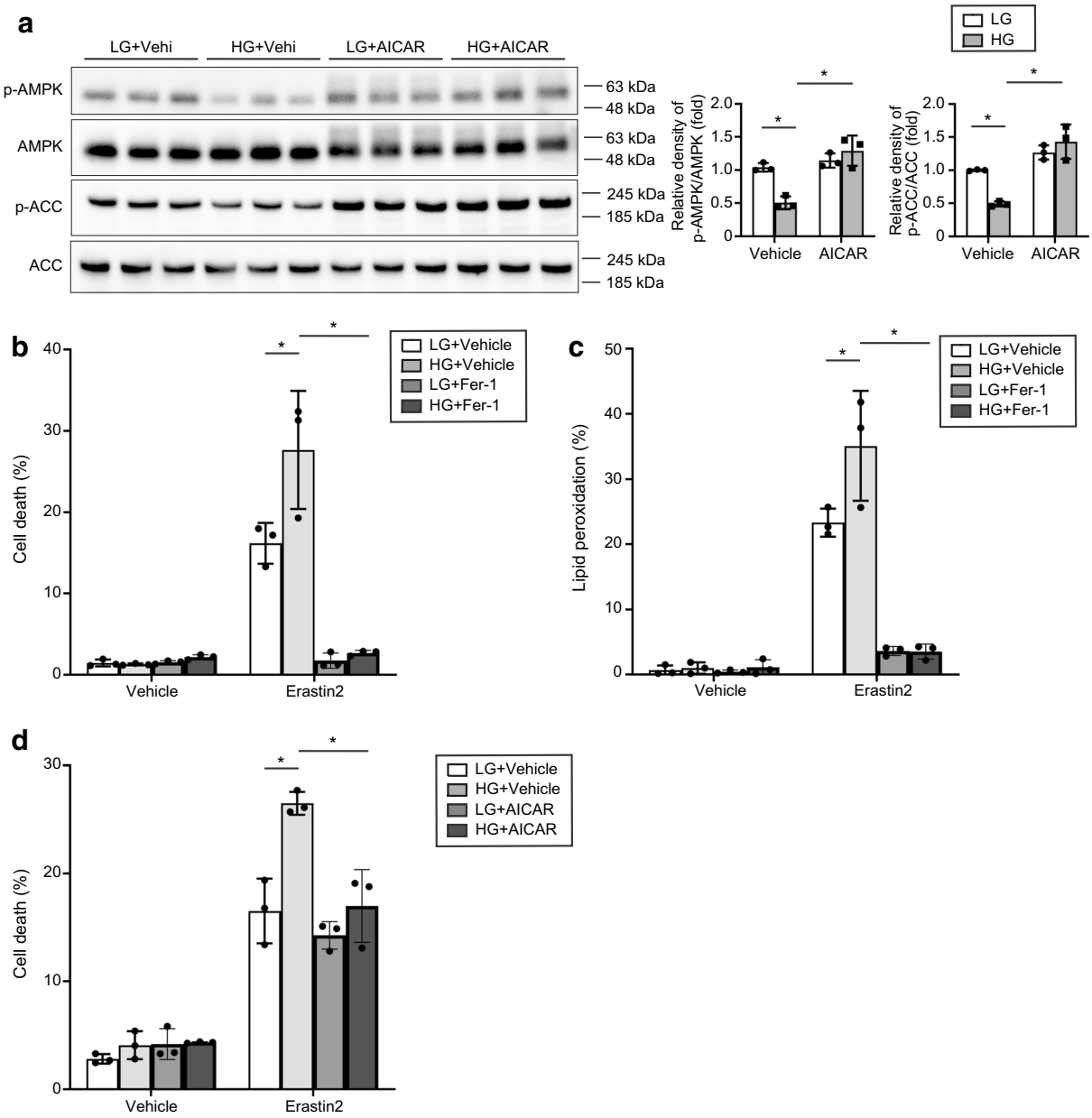

Fig. 6 HG-induced inactivation of AMPK promotes ferroptosis in PTECs. (**a**) Representative western blot images of p-AMPK, total AMPK, p-ACC and total ACC in cultured PTECs incubated with LG or HG, with or without AICAR (n=3 per group). (**b**, **c**) Quantification of cell death (**b**) and lipid peroxidation (**c**) in cultured PTECs incubated with LG or HG, with or without Fer-1, and treated with or without 1 μmol/l erastin2 for 24 h. (**d**) Quantification of cell death in cultured PTECs incubated with LG or HG, with or without AICAR, and treated with or without 1 μmol/l erastin2 for 24 h. Data are means ± SD. Statistically significant differences are indicated by asterisks (p<0.05). All images are representative of multiple experiments. Vehi, vehicle

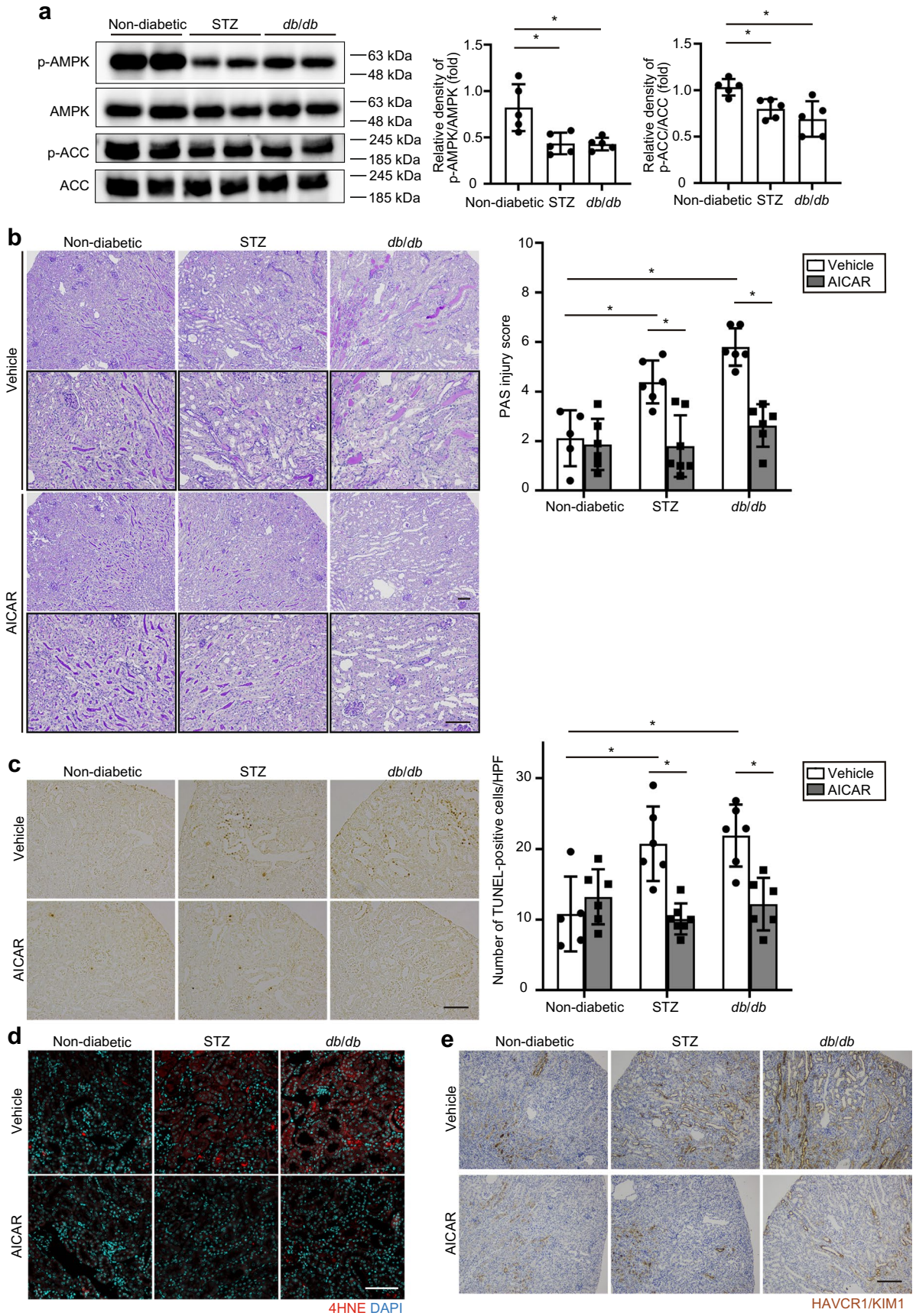
a
Non-diabetic
STZ
db/db
p-AMPK
AMPK
p-ACC
ACC
63 kDa
48 kDa
63 kDa
48 kDa
245 kDa
185 kDa
245 kDa
185 kDa
Relative density of p-AMPK/AMPK (fold)
Relative density of p-ACC/ACC (fold)
b
Vehicle
AICAR
PAS injury score
c
Number of TUNEL-positive cells/HPF
d
4HNE DAPI
e
HAVCR1/KIM1

◂**Fig. 7** AMPK activation attenuates vulnerability to ischaemia–reperfusion injury in diabetic mice. (**a**) Representative western blot images of p-AMPK, total AMPK, p-ACC and total ACC in kidney lysates from non-diabetic, STZ-treated and *db*/*db* mice (n=5 per group). (**b**, **c**) Representative images of PAS staining (**b**) and TUNEL staining (**c**) of ischaemia–reperfusion-injured renal cortices from non-diabetic, STZ-treated and *db*/*db* mice with or without AICAR treatment, 2 days after unilateral ischaemia–reperfusion injury (n=5–7 per group). PAS injury scores are presented. TUNEL-positive PTECs were quantified across at least ten high-power fields (HPF) (×200). (**d**, **e**) Representative immunofluorescence images of 4HNE (**d**) and immunohistochemical images of HAVCR1/KIM1 (**e**) in the ischaemia–reperfusion-injured renal cortex. Scale bars, 100 μm. Data are means ± SD. Statistically significant differences are indicated by asterisks (p<0.05). All images are representative of multiple experiments. PAS, periodic acid–Schiff

indicator in kidney tissue. Moreover, the presence of lipid peroxides in PTECs where ferroptosis has not yet occurred suggests that ferroptosis may occur when subsequent triggers drive lipid peroxides beyond a lethal threshold. Thus, lipid peroxide accumulation may represent a primed state of ferroptosis susceptibility in human kidneys.

A variety of cancer cell lines have been reported to exhibit autophagy-driven ferroptosis. However, in contrast to previous reports [21–25], our findings demonstrate that autophagy confers resistance to ferroptosis in PTECs. This discrepancy may stem from differences in cell type. For instance, metabolic profiles vary between cells: primary renal PTECs, as used in our study, rely predominantly on fatty acid oxidation [45], whereas cancer cell lines depend primarily on glycolysis, probably due to mitochondrial dropout [46]. This metabolic divergence may influence the effect of *Atg5* knockout on ferroptosis susceptibility, as ferroptosis is regulated by cellular metabolic processes involving lipid peroxidation, including redox balance, iron handling, mitochondrial function and the metabolism of amino acids, lipids and sugars [10].

We demonstrated that autophagy suppresses ferroptosis by reducing mitochondrial ROS in PTECs. Recent studies have shown that mitochondria play diverse, context-dependent roles in modulating ferroptosis sensitivity [47, 48]. In the context of autophagy, one study reported that mitophagy protects against ferroptosis by downregulating mitochondrial ROS [49]. PTECs are mitochondria-rich and derive their energy primarily from oxidative phosphorylation. In mitochondria-rich PTECs, mitochondrial ROS are inevitably produced as byproducts of oxidative phosphorylation, making it essential to maintain low mitochondrial ROS levels. Autophagy supports this by facilitating the clearance of damaged mitochondria through mitophagy and macroautophagy, thereby preventing ROS accumulation and preserving mitochondrial quality [15, 50]. Indeed, mitophagy-deficient mice (*pink1* knockout or *park2* knockout) exhibit increased susceptibility to ischaemia–reperfusion injury [51]. These findings suggest that autophagy mitigates mitochondrial ROS accumulation and thereby inhibits ferroptosis in PTECs.

HG-induced AMPK inactivation, together with ACC dephosphorylation, sensitised cells to ferroptotic cell death. The role of AMPK in ferroptosis remains controversial [52, 53]; however, one study showed that energy stress activates AMPK, which phosphorylates and inactivates ACC, thereby suppressing polyunsaturated fatty acid

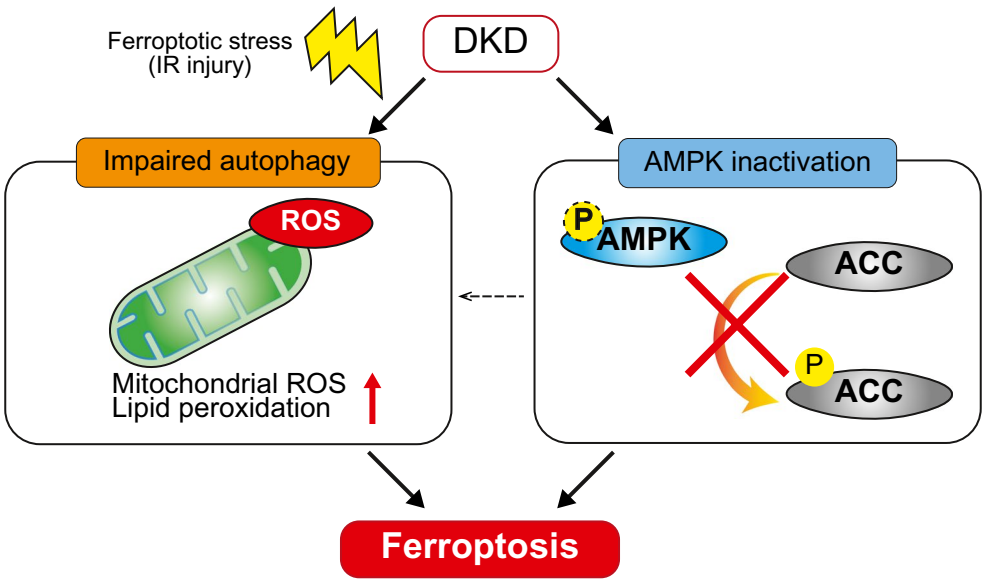

Fig. 8 Schematic illustration of the findings of this study. DKD leads to autophagy impairment and inactivation of AMPK and ACC signalling. Impaired autophagy sensitises PTECs to ferroptotic cell death via mitochondrial ROS accumulation. Disruption of the AMPK–ACC axis further increases susceptibility to ferroptosis. IR, ischaemia–reperfusion

biosynthesis and inhibiting ferroptosis. In light of these insights, HG-induced disruption of AMPK and ACC may enhance polyunsaturated fatty acid biosynthesis, increasing susceptibility to ferroptosis in PTECs. Conversely, activation of AMPK and ACC through AICAR treatment may reduce polyunsaturated fatty acid biosynthesis, thereby promoting resistance to ferroptosis in PTECs. Furthermore, our findings demonstrate that AICAR enhances autophagic activity in HG-treated PTECs, suggesting that AMPK activation may confer resistance to ferroptosis in PTECs by improving autophagy.

Ferroptosis has garnered attention as a potential target in cancer therapy [54]. If ferroptosis inducers are applied clinically, renal tubules that are highly vulnerable to ferroptosis may be at risk of injury. Our findings suggest that autophagy activation may mitigate such effects, protecting normal cells while allowing ferroptosis induction in cancer cells. Although prior studies indicated that autophagy activation sensitises cancer cells to ferroptosis [21–25], our data suggest that autophagy may protect renal tubules from ferroptotic injury. Thus, in therapeutic contexts, autophagy activation may offer systemic protective benefits.

Our study explains why diabetic individuals with elevated blood glucose levels are susceptible to AKI, but it may not fully account for why individuals with well-controlled glucose levels also develop AKI, which is a limitation. However, diabetic patients are known to experience glycaemic legacy effects, in which prior hyperglycaemia – even after subsequent glucose normalisation – causes lasting detrimental effects through mechanisms such as epigenetic modifications [55]. These effects may contribute to the persistent impairment of autophagy and AMPK inactivation in PTECs of diabetic individuals. Furthermore, while HbA_{1c} levels below 53 mmol/mol (7.0%) are generally considered indicative of good glycaemic management, patients with HbA_{1c} levels around 42 mmol/mol (6%) still have higher blood glucose levels compared with healthy individuals, which may influence AMPK activity and autophagy status. Consistently, for our human kidney biopsy samples, individuals in the DKD group had a mean HbA_{1c} of 49.4 mmol/mol (6.67%) which was higher than that in the non-DKD group but still within the range of good glycaemic management, yet still exhibited impaired autophagy and AMPK inactivation in PTECs.

In conclusion, we demonstrate that defective autophagy and AMPK inactivation enhance susceptibility to ferroptosis in DKD. These findings highlight new opportunities for therapeutic interventions in AKI associated with DKD.

Supplementary Information The online version contains peer-reviewed but unedited supplementary material available at https://doi.org/10.1007/s00125-025-06612-2.

Acknowledgements We thank T. Matsusaka and F. Niimura (Tokai University School of Medicine) for providing the KAP-Cre mice, N. Mizushima (University of Tokyo) for the *Atg5*$^{F/F}$ mice, T. Michigami (Osaka Medical Center and Research Institute) for the LRP2/MEGALIN antibody, and N. Horimoto (The University of Osaka) for technical assistance.

Data availability All data are available from the authors upon reasonable request.

Funding This work was supported by Grants-in-Aid for Scientific Research from the Ministry of Education, Culture, Sports, Science and Technology of Japan (25K19490 to SM, 23K07671 to TY, and 24K02467 to YI), the Osaka Kidney Bank (to SM) and the Japan Diabetes Foundation (to SM), and by the Uehara Memorial Foundation, the G-7 Scholarship Foundation, the Kanae Foundation for the Promotion of Medical Science, the MSD Life Science Foundation, the Japan Diabetes Foundation/Nippon Boehringer Ingelheim Co. Ltd & Eli Lilly Japan K.K., the Japan Diabetes Foundation/Costco Wholesale Japan Ltd and the Ichiro Kanehara Foundation (to TY). This work was partially supported by Nippon Boehringer Ingelheim Co. Ltd and Eli Lilly Japan K.K. through a commissioned research agreement. Nippon Boehringer Ingelheim Co. Ltd and Eli Lilly Japan K.K. had no role in the design, analysis or interpretation of the results in this study.

Authors' relationships and activities The authors declare that there are no relationships or activities that might bias, or be perceived to bias, their work.

Contribution statement SMa and TY were responsible for study conception, investigation, data acquisition and analysis, and manuscript drafting and reviewing. YT was responsible for study conception and manuscript drafting and reviewing. AT, TNH, JM, SS, HY, JN, HK and TK contributed to data analysis and interpretation. YI, IM, YT, SMi and MY contributed to review and editing of the manuscript. All authors interpreted the data, critically revised the manuscript and approved the final version for submission. SMa, TY and YI are the guarantors of this work.

References

1. GBD 2021 Diabetes Collaborators (2023) Global, regional, and national burden of diabetes from 1990 to 2021, with projections of prevalence to 2050: a systematic analysis for the Global Burden

of Disease Study 2021. Lancet 402(10397):203–234. https://doi.org/10.1016/S0140-6736(23)01301-6
2. Oshima M, Shimizu M, Yamanouchi M et al (2021) Trajectories of kidney function in diabetes: a clinicopathological update. Nat Rev Nephrol 17(11):740–750. https://doi.org/10.1038/s41581-021-00462-y
3. Xu Y, Surapaneni A, Alkas J et al (2020) Glycemic control and the risk of acute kidney injury in patients with type 2 diabetes and chronic kidney disease: parallel population-based cohort studies in U.S. and Swedish routine care. Diabetes Care 43(12):2975–2982. https://doi.org/10.2337/dc20-1588
4. James MT, Grams ME, Woodward M et al (2015) A meta-analysis of the association of estimated gfr, albuminuria, diabetes mellitus, and hypertension with acute kidney injury. Am J Kidney Dis 66(4):602–612. https://doi.org/10.1053/j.ajkd.2015.02.338
5. Mo M, Huang Z, Gao T et al (2022) Development and validation of short-term renal prognosis prediction model in diabetic patients with acute kidney injury. Diabetol Metab Syndr 14(1):197. https://doi.org/10.1186/s13098-022-00971-1
6. Lo LJ, Go AS, Chertow GM et al (2009) Dialysis-requiring acute renal failure increases the risk of progressive chronic kidney disease. Kidney Int 76(8):893–899. https://doi.org/10.1038/ki.2009.289
7. Ishani A, Xue JL, Himmelfarb J et al (2009) Acute kidney injury increases risk of ESRD among elderly. J Am Soc Nephrol 20(1):223–228. https://doi.org/10.1681/ASN.2007080837
8. Hoste EAJ, Kellum JA, Selby NM et al (2018) Global epidemiology and outcomes of acute kidney injury. Nat Rev Nephrol 14(10):607–625. https://doi.org/10.1038/s41581-018-0052-0
9. Dixon SJ, Lemberg KM, Lamprecht MR et al (2012) Ferroptosis: an iron-dependent form of nonapoptotic cell death. Cell 149(5):1060–1072. https://doi.org/10.1016/j.cell.2012.03.042
10. Jiang X, Stockwell BR, Conrad M (2021) Ferroptosis: mechanisms, biology and role in disease. Nat Rev Mol Cell Biol. https://doi.org/10.1038/s41580-020-00324-8
11. Friedmann Angeli JP, Schneider M, Proneth B et al (2014) Inactivation of the ferroptosis regulator Gpx4 triggers acute renal failure in mice. Nat Cell Biol 16(12):1180–1191. https://doi.org/10.1038/ncb3064
12. Linkermann A, Skouta R, Himmerkus N et al (2014) Synchronized renal tubular cell death involves ferroptosis. Proc Natl Acad Sci USA 111(47):16836–16841. https://doi.org/10.1073/pnas.1415518111
13. Maremonti F, Meyer C, Linkermann A (2022) Mechanisms and models of kidney tubular necrosis and nephron loss. J Am Soc Nephrol 33(3):472–486. https://doi.org/10.1681/ASN.2021101293
14. Wang H, Liu D, Zheng B et al (2023) Emerging role of ferroptosis in diabetic kidney disease: molecular mechanisms and therapeutic opportunities. Int J Biol Sci 19(9):2678–2694. https://doi.org/10.7150/ijbs.81892
15. Mizushima N, Levine B (2020) Autophagy in human diseases. N Engl J Med 383(16):1564–1576. https://doi.org/10.1056/NEJMra2022774
16. Kimura T, Takabatake Y, Takahashi A et al (2011) Autophagy protects the proximal tubule from degeneration and acute ischemic injury. J Am Soc Nephrol 22(5):902–913. https://doi.org/10.1681/ASN.2010070705
17. Takahashi A, Kimura T, Takabatake Y et al (2012) Autophagy guards against cisplatin-induced acute kidney injury. Am J Pathol 180(2):517–525. https://doi.org/10.1016/j.ajpath.2011.11.001
18. Xie Y, Kang R, Sun X et al (2015) Posttranslational modification of autophagy-related proteins in macroautophagy. Autophagy 11(1):28–45. https://doi.org/10.4161/15548627.2014.984267
19. Sakai S, Yamamoto T, Takabatake Y et al (2019) Proximal tubule autophagy differs in type 1 and 2 diabetes. J Am Soc Nephrol 30(6):929–945. https://doi.org/10.1681/ASN.2018100983
20. Li S, Liao Z, Yin H et al (2023) G3BP1 coordinates lysophagy activity to protect against compression-induced cell ferroptosis during intervertebral disc degeneration. Cell Prolif 56(3):e13368. https://doi.org/10.1111/cpr.13368
21. Liu J, Kuang F, Kroemer G, Klionsky DJ, Kang R, Tang D (2020) Autophagy-dependent ferroptosis: machinery and regulation. Cell Chem Biol 27(4):420–435. https://doi.org/10.1016/j.chembiol.2020.02.005
22. Hou W, Xie Y, Song X et al (2016) Autophagy promotes ferroptosis by degradation of ferritin. Autophagy 12(8):1425–1428. https://doi.org/10.1080/15548627.2016.1187366
23. Bai Y, Meng L, Han L et al (2019) Lipid storage and lipophagy regulates ferroptosis. Biochem Biophys Res Commun 508(4):997–1003. https://doi.org/10.1016/j.bbrc.2018.12.039
24. Wu Z, Geng Y, Lu X et al (2019) Chaperone-mediated autophagy is involved in the execution of ferroptosis. Proc Natl Acad Sci USA 116(8):2996–3005. https://doi.org/10.1073/pnas.1819728116
25. Yang M, Chen P, Liu J et al (2019) Clockophagy is a novel selective autophagy process favoring ferroptosis. Sci Adv 5(7):eaaw2238. https://doi.org/10.1126/sciadv.aaw2238
26. Huynh C, Ryu J, Lee J, Inoki A, Inoki K (2022) Nutrient-sensing mTORC1 and AMPK pathways in chronic kidney diseases. Nat Rev Nephrol. https://doi.org/10.1038/s41581-022-00648-y
27. Lee MJ, Feliers D, Mariappan MM et al (2007) A role for AMP-activated protein kinase in diabetes-induced renal hypertrophy. Am J Physiol Renal Physiol 292(2):F617–F627. https://doi.org/10.1152/ajprenal.00278.2006
28. Kitada M, Kume S, Imaizumi N, Koya D (2011) Resveratrol improves oxidative stress and protects against diabetic nephropathy through normalization of Mn-SOD dysfunction in AMPK/SIRT1-independent pathway. Diabetes 60(2):634–643. https://doi.org/10.2337/db10-0386
29. Herzig S, Shaw RJ (2018) AMPK: guardian of metabolism and mitochondrial homeostasis. Nat Rev Mol Cell Biol 19(2):121–135. https://doi.org/10.1038/nrm.2017.95
30. Yamamoto T, Takabatake Y, Kimura T et al (2016) Time-dependent dysregulation of autophagy: implications in aging and mitochondrial homeostasis in the kidney proximal tubule. Autophagy 12(5):801–813. https://doi.org/10.1080/15548627.2016.1159376
31. Yamamoto T, Takabatake Y, Takahashi A et al (2017) High-fat diet-induced lysosomal dysfunction and impaired autophagic flux contribute to lipotoxicity in the kidney. J Am Soc Nephrol 28(5):1534–1551. https://doi.org/10.1681/ASN.2016070731
32. Yamamoto T, Takabatake Y, Minami S et al (2021) Eicosapentaenoic acid attenuates renal lipotoxicity by restoring autophagic flux. Autophagy 17(7):1700–1713. https://doi.org/10.1080/15548627.2020.1782034
33. Rueden CT, Schindelin J, Hiner MC et al (2017) Image J2: ImageJ for the next generation of scientific image data. BMC Bioinformatics 18(1):529. https://doi.org/10.1186/s12859-017-1934-z
34. Mootha VK, Lindgren CM, Eriksson KF et al (2003) PGC-1α-responsive genes involved in oxidative phosphorylation are coordinately downregulated in human diabetes. Nat Genet 34(3):267–273. https://doi.org/10.1038/ng1180
35. Subramanian A, Tamayo P, Mootha VK et al (2005) Gene set enrichment analysis: a knowledge-based approach for interpreting genome-wide expression profiles. Proc Natl Acad Sci USA 102(43):15545–15550. https://doi.org/10.1073/pnas.0506580102
36. Wu T, Hu E, Xu S et al (2021) clusterProfiler 4.0: a universal enrichment tool for interpreting omics data. Innovation

(Cambridge) 2(3):100141. https://doi.org/10.1016/j.xinn.2021.100141
37. Matsui I, Ito T, Kurihara H, Imai E, Ogihara T, Hori M (2007) Snail, a transcriptional regulator, represses nephrin expression in glomerular epithelial cells of nephrotic rats. Lab Invest 87(3):273–283. https://doi.org/10.1038/labinvest.3700518
38. Ni L, Yuan C, Wu X (2022) Targeting ferroptosis in acute kidney injury. Cell Death Dis 13(2):182. https://doi.org/10.1038/s41419-022-04628-9
39. Bhargava P, Schnellmann RG (2017) Mitochondrial energetics in the kidney. Nat Rev Nephrol 13(10):629–646. https://doi.org/10.1038/nrneph.2017.107
40. McWilliams TG, Prescott AR, Allen GF et al (2016) mito-QC illuminates mitophagy and mitochondrial architecture in vivo. J Cell Biol 214(3):333–345. https://doi.org/10.1083/jcb.201603039
41. Picca A, Faitg J, Auwerx J, Ferrucci L, D'Amico D (2023) Mitophagy in human health, ageing and disease. Nat Metab 5(12):2047–2061. https://doi.org/10.1038/s42255-023-00930-8
42. Prime TA, Forkink M, Logan A et al (2012) A ratiometric fluorescent probe for assessing mitochondrial phospholipid peroxidation within living cells. Free Radic Biol Med 53(3):544–553. https://doi.org/10.1016/j.freeradbiomed.2012.05.033
43. Garcia D, Shaw RJ (2017) AMPK: mechanisms of cellular energy sensing and restoration of metabolic balance. Mol Cell 66(6):789–800. https://doi.org/10.1016/j.molcel.2017.05.032
44. Dixon SJ, Olzmann JA (2024) The cell biology of ferroptosis. Nat Rev Mol Cell Biol 25(6):424–442. https://doi.org/10.1038/s41580-024-00703-5
45. Hammoud S, Kern J, Mukherjee S et al (2025) Assays to enhance metabolic phenotyping in the kidney. Am J Physiol Renal Physiol 328(4):F563–F577. https://doi.org/10.1152/ajprenal.00232.2024
46. Kondoh H (2008) Cellular life span and the Warburg effect. Exp Cell Res 314(9):1923–1928. https://doi.org/10.1016/j.yexcr.2008.03.007
47. Gao M, Yi J, Zhu J et al (2019) Role of mitochondria in ferroptosis. Mol Cell 73(2):354-363 e353. https://doi.org/10.1016/j.molcel.2018.10.042
48. Mao C, Liu X, Zhang Y et al (2021) DHODH-mediated ferroptosis defence is a targetable vulnerability in cancer. Nature. https://doi.org/10.1038/s41586-021-03539-7
49. Yamashita SI, Sugiura Y, Matsuoka Y et al (2024) Mitophagy mediated by BNIP3 and NIX protects against ferroptosis by downregulating mitochondrial reactive oxygen species. Cell Death Differ 31(5):651–661. https://doi.org/10.1038/s41418-024-01280-y
50. Palikaras K, Lionaki E, Tavernarakis N (2018) Mechanisms of mitophagy in cellular homeostasis, physiology and pathology. Nat Cell Biol 20(9):1013–1022. https://doi.org/10.1038/s41556-018-0176-2
51. Tang C, Han H, Yan M et al (2018) PINK1–PRKN/PARK2 pathway of mitophagy is activated to protect against renal ischemia-reperfusion injury. Autophagy 14(5):880–897. https://doi.org/10.1080/15548627.2017.1405880
52. Zhao Y, Li M, Yao X et al (2020) HCAR1/MCT1 regulates tumor ferroptosis through the lactate-mediated AMPK–SCD1 activity and its therapeutic implications. Cell Rep 33(10):108487. https://doi.org/10.1016/j.celrep.2020.108487
53. Song X, Zhu S, Chen P et al (2018) AMPK-mediated BECN1 phosphorylation promotes ferroptosis by directly blocking system Xc^- activity. Curr Biol 28(15):2388-2399 e2385. https://doi.org/10.1016/j.cub.2018.05.094
54. Nakamura T, Conrad M (2024) Exploiting ferroptosis vulnerabilities in cancer. Nat Cell Biol 26(9):1407–1419. https://doi.org/10.1038/s41556-024-01425-8
55. Lachin JM, Nathan DM, DCCT/EDIC Research Group (2021) Understanding metabolic memory: the prolonged influence of glycemia during the Diabetes Control and Complications Trial (DCCT) on future risks of complications during the Study of the Epidemiology of Diabetes Interventions and Complications (EDIC). Diabetes Care 44(10):2216–2224. https://doi.org/10.2337/dc20-3097